Theor Chem Acc (2010) 125:387–396
DOI 10.1007/s00214-009-0658-1

REGULAR ARTICLE

# Competing gas-phase fragmentation pathways of asparagine-, glutamine-, and lysine-containing protonated dipeptides

**Christian Bleiholder · Béla Paizs**

Received: 1 August 2009 / Accepted: 6 October 2009 / Published online: 11 November 2009


**Abstract** The fragmentation chemistry of protonated H–Val–Asn–OH, H–Val–Gln–OH and H–Val–Lys–OH is investigated in this work by means of modeling and density functional theory calculations. Former experimental studies indicate that the ratio of $a_1$ and $y_1$ ions cannot be explained by considering the proton affinities of the corresponding dissociating species on the $a_1$–$y_1$ pathway, while the fragmentation of other dipeptides can be understood in this way. We demonstrate that considering the correct PA value for H–Asn–OH eliminates the deviation observed for H–Val–Asn–OH. The larger than expected $a_1/y_1$ ratio of H–Val–Gln–OH is explained by considering the dissociation kinetics of the proton-bound dimers formed on the $a_1$–$y_1$ pathway and competition of the deamidation and $a_1$–$y_1$ channels. For H–Val–Lys–OH, it is proposed that $a_1$ ions are indeed formed from one of the primary products, protonated H–Val–Cap–OH.

**Keywords** Protonated peptides · Peptide fragmentation · *y* ion · *a* ion · Reaction mechanism · Quantum chemistry · Mass spectrometry

Dedicated to Prof. Sándor Suhai on the occasion of his 65th birthday and published as part of the Suhai Festschrift Issue.

C. Bleiholder · B. Paizs (✉)
Department of Molecular Biophysics,
German Cancer Research Center,
Im Neuenheimer Feld 580, 69120 Heidelberg, Germany
e-mail: B.Paizs@dkfz.de; B.Paizs@dkfz-heidelberg.de

*Present Address:*
C. Bleiholder
Department of Chemistry and Biochemistry,
University of California, Santa Barbara,
CA 93106-9510, USA

## 1 Introduction

Fast and reliable identification of proteins is of great importance in modern biomedical research. The most widespread used protein identification strategy in the exploding field of proteomics is based on tandem mass spectrometry (MS/MS) of peptides [1] produced by enzymatic digestions of proteins. In these experiments, peptides are ionized by protonation and the resulting ions are excited and fragmented by collisions (CID, collision-induced dissociation) with inert gas atoms/molecules. The product ion spectra of protonated peptides are usually assigned using bioinformatics algorithms, which compare the experimentally observed fragmentation patterns to theoretical (*in silico*) MS/MS spectra predicted for peptide sequences in databases using various fragmentation models [2]. The goodness of the predicted *in silico* spectra is one of the key factors determining the reliability of protein identifications in proteomics. Therefore, much research is currently devoted to improving existing strategies [3].

Most fragmentation models implemented in the current sequencing software consider only the first dimension of mass spectra (mass to charge ratio (*m*/*z*) of fragment ions) and apply uniform fragment ion abundance distributions in generating in silico spectra. The various fragmentation models differ from each other even in the way they make use of various fragment ions that are commonly observed in product ion spectra of protonated peptides. While these spectra contain a variety of distinct fragment ion types, most algorithms use only the major backbone fragmentation series (*b*, *a* and *y,* for the nomenclature see Refs. [4, 5]), and only a few consider additional information such as loss of small neutrals as ammonia or water. Peptide and protein sequencing could no doubt be improved by implementing fragmentation models, which predict the

observed fragment ions and their relative abundances better.

Bursey and Harrison have observed [6–8] that some relative fragment ion abundances in product ion spectra of protonated peptides can be understood by considering simple thermodynamics rules. For example, Harrison and co-workers studied [8] the fragmentation of the H–Val–Xxx–OH (Xxx includes Ala, Ser, Asp, Val, Leu, Phe, Tyr, Met, Glu, Trp) series of peptides and found a linear relationship between the logarithm of the $y_1/a_1$ fragment ion abundance ratio and the proton affinity (PA) of the varied amino acid (the $a_1$ fragment is protonated Val imine ($NH_2^+$=CHCHMe$_2$) and the $y_1$ fragment is protonated H–Xxx–OH for the H–Val–Xxx–OH series).

The linearity of the $\log(y_1/a_1)$ versus PA(Xxx) relationship could be explained based on detailed computational studies of the $a_1$–$y_1$ pathway forming the $a_1$ and $y_1$ fragments [9, 10]. Ionization by protonation using mild ionization techniques leads to the energetically most favored protonated peptide structure. For peptides lacking basic amino acids (arginine, lysine and histidine), this means protonation at the N-terminal amino group. Since such structures do not directly fragment, intermolecular proton transfer reactions populate more reactive protonation forms [11] (Scheme 1). Provided enough energy is deposited into the peptide ions, the amide oxygen or nitrogen protonated species become populated (Scheme 1). The latter can fragment directly by concerted cleavage of the protonated amide and the $C_\alpha$–$C_{carbonyl}$ bonds resulting in a protonated trimer of the N-terminal imine, the C-terminal amino acid fragment and CO. After loss of the weakly bonded CO, a proton-bound dimer (Scheme 1) of the imine and the H–Xxx–OH amino acid is formed. Under low-energy conditions, the lifetime of this dimer is long enough so that the various proton-bound dimer isomers can interconvert [12] and proton transfers can take place between the imine and H-Xxx-OH. As a result, there are two exit channels through which the proton-bound dimer can dissociate to give either $a_1$ or $y_1$ ions (Scheme 1). The actual dissociation kinetics of the proton-bound dimer is rather complicated [13–15] and depends on various physicochemical properties, such as the internal energy distribution and the PA of the respective monomers. However, it was shown that the resulting relative ion intensities can be approximated by a simple linear free energy relationship:

$$\log(\text{C-term/N-term}) \sim (\text{PA}_{\text{C-term}} - \text{PA}_{\text{N-term}})/\text{RT}_{\text{eff}}. \quad (1)$$

Here, C-term/N-term is the ratio of the C-terminal ($y_1$) and N-terminal ($a_1$) ion abundances, $PA_{C\text{-term}}$ and $PA_{N\text{-term}}$ are the proton affinities of the C- and N-terminal fragments (NH = CHCHMe$_2$ and H–Xxx–OH for the H–Val–Xxx–OH

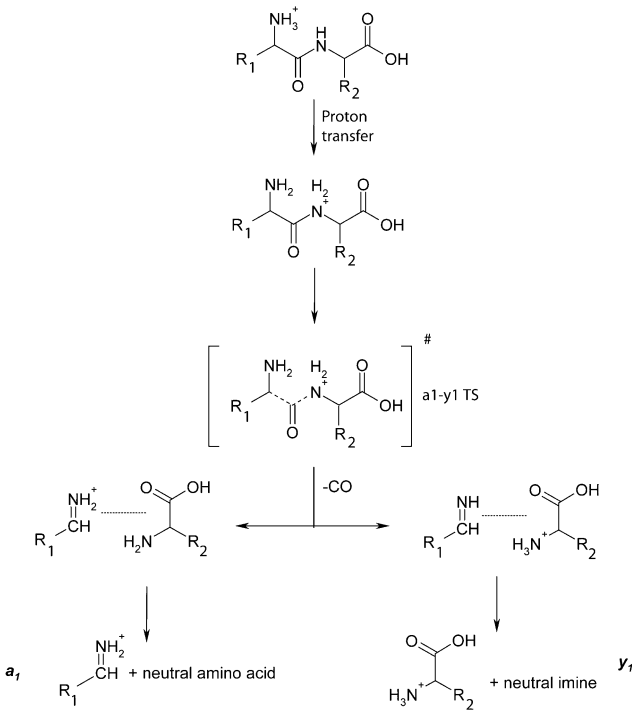


**Scheme 1** Overview of the major steps on the $a_1$–$y_1$ pathway including proton mobilization, cleavage of the protonated amide bond, formation and dissociation of the proton-bound dimers of the N- and C-terminal fragments

series), and $T_{eff}$ denotes the "effective temperature". Note that Eq. (1) holds only if two dissociation channels of the proton-bound dimer exist and the two exit channels involve barrier-less dissociations and have similar dissociation entropies. Because these preconditions are not strictly met in a general case, the above equation should be considered as a semi-quantitative estimate only.

Equation (1) explains Harrison's observation [8] that the logarithm of the $y_1/a_1$ fragment ion abundance ratio is a linear function of the PA of the varied amino acid for the H–Val–Xxx–OH (Xxx here includes Ala, Ser, Asp, Val, Leu, Phe, Tyr, Met, Glu, Trp) peptide series. For this series, the PA of the N-terminal fragment ($NH_2$ = CHCHMe$_2$) is fixed and only the PA of the C-terminal fragment changes as Xxx is varied. Furthermore, this approach was applied successfully by Wesdemiotis and co-workers [16] to rationalize the fragmentation chemistry of dipeptide isomers H–Xxx–Yyy–OH and H–Yyy–Xxx–OH. However, Harrison also noted [8] that Eq. (1) does not satisfactorily explain the $y_1/a_1$ ratio of the dipeptides H–Val–Asn–OH, H–Val–Gln–OH and H–Val–Lys–OH, respectively. The reasons for this 'unusual' fragmentation behavior are explored in detail in the present study using theoretical tools involving molecular dynamics and quantum chemical calculations.

## 2 Computational details

To scan the potential energy surface (PES) of protonated H–Val–Asn–OH, H–Val–Gln–OH and H–Val–Lys–OH, we applied our recently developed conformational search engine [17–22] devised specifically to deal with protonated peptides. These calculations started with molecular dynamics simulations on various protonated forms of the above dipeptides using the Discover program (Biosym Technologies, San Diego, CA, USA) in conjunction with the AMBER force field [23] modified by us to manage amide nitrogen and oxygen protonated species. During the dynamics, structures were regularly saved for further refinement by full geometry optimization using the same force fields. In the next step of the scan, these structures were analyzed by our conformer family search program. This program is able to group optimized structures into families for which the most important characteristic torsion angles of the molecule are similar. The most stable species in the families were then fully optimized at the HF/3-21G, B3LYP/6-31G(d) and finally at the B3LYP/6-31 + G(d,p) levels of theory.

Transition structures (TS) were determined at the B3LYP/6-31G(d) and B3LYP/6-31 + G(d,p) levels of theory. All TSs were checked by using intrinsic reaction path calculations (IRC) to unambiguously define which minima were connected by the TS investigated. Similarly for the species belonging to the various protonation sites and transition structures, post-reaction complexes and proton-bound dimers were fully optimized at the B3LYP/6-31G(d) and B3LYP/6-31 + G(d,p) levels of theory. Relative energies were calculated with respect to the most stable species of the investigated protonated dipeptides by using B3LYP/6-31 + G(d,p) total energies and B3LYP/6-31G(d) zero-point energy corrections (ZPE). For all quantum chemical calculations, the Gaussian [24] program was used.

## 3 Results and discussion

In a recent study [25], we have shown that the PA scale used by Harrison [26] to plot the $\log(y_1/a_1)$ [8] versus PA(H–Xxx–OH) relationship was not fully consistent and suggested new values for H–Asn–OH and H–Gln–OH. In Fig. 1, Harrison's $\log(a_1/y_1)$ values for the H–Val–Xxx–OH series (Xxx involves Ala, Ser, Asp, Val, Leu, Phe, Tyr, Met, Glu, Trp, Asn, Gln, Pro, and Lys) [8] are plotted against the revised amino acid PAs [25, 26]. The linear free energy relationship (LFER) observed originally by Harrison et al. [8] is reproduced ($R = 0.983$). The revised PA of H–Asn–OH places the H–Val–Xxx–OH $\log(a_1/y_1)$ value close to the expected $a_1/y_1$ ratio, suggesting that the

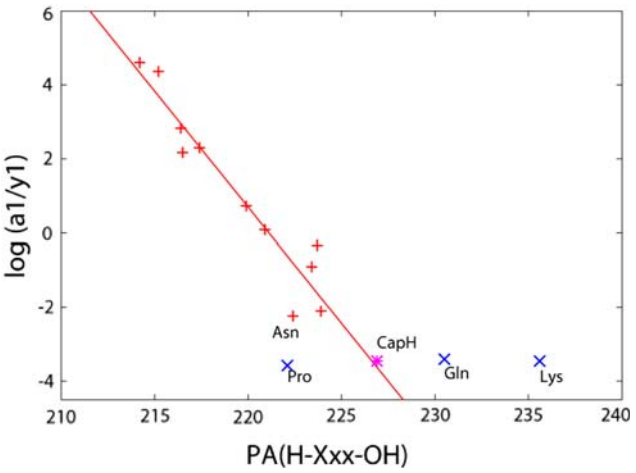


**Fig. 1** $\log(a_1/y_1)$ [8] as a function of the revised amino acid PA values [25, 26] for the H–Val–Xxx–OH peptide series. Peptides with $\log(a_1/y_1)$ values deviating from the expected linear relationship are indicated in *blue*

fragmentation of this dipeptide is "usual" and the $a_1/y_1$ ratio can be approximated by Eq. (1). On the other hand, the $a_1/y_1$ ratios of H–Val–Gln–OH and H–Val–Lys–OH clearly deviate from the values indicated by Eq. (1) and the corresponding PA data. A common characteristic of these deviations is that the observed $a_1$ abundances are higher than those expected from Eq. (1). The PA of i-pr-imine (221.7 kcal/mol) is much lower than those of H–Gln–OH (230.5 kcal/mol) and H–Lys–OH (235.8 kcal/mol) [25, 26]. Such large differences in PA suggest that virtually no $a_1$ ions should be observed; however, the experimental $a_1$:$y_1$ ratio is $\sim$1:30 in both cases.

### 3.1 Fragmentation pathways of protonated H–Val–Asn–OH and H–Val–Gln–OH

The product ion spectra [8] of protonated H–Val–Asn–OH and H–Val–Gln–OH contain abundant $a_1$ (10.7 and 3.33%), $y_1$ (100 and 100%) and $[MH–NH_3]^+$ (105 and 95.0%) ions. This indicates that protonated H–Val–Asn–OH and H–Val–Gln–OH fragments are present in two competing pathways, one leading to $[MH–NH_3]^+$ and another leading to $a_1$ and $y_1$ ions. The deamidation pathways of some Gln-containing dipeptides (H–Xxx–Gln–OH, Xxx involves Gly, Ala, and Val) have been investigated by Harrison [27] using low-energy CID and energy-resolved MS/MS experiments. Recently, Armentrout and co-workers have investigated the deamidation pathways of protonated asparagine [28]. These studies demonstrated that $NH_3$ was lost from the side chain amide functionality.

The terminal amino group is the most favored protonation site for both H–Val–Asn–OH and H–Val–Gln–OH (Table 1, Scheme 2). Both the $a_1$–$y_1$ and deamidation

**Table 1** Relative energies (kcal/mol, corrected for ZPE and calculated with respect to the global minimum on the corresponding PES) of various structures on the PESs of protonated H–Val–Asn–OH, H–Val–Gln–OH and H–Val–Lys–OH

| | H–Val–Asn–OH | H–Val–Gln–OH | H–Val–Lys–OH |
|---|---|---|---|
| Protonation sites | | | |
| N-terminus | 0.0 | 0.0 | 3.4 |
| $O_{amide}$ | 2.0 | 1.1 | 11.3 |
| $N_{amide}$ | 15.0 | 12.9 | 18.5 |
| $O_{side\ chain}$ | 11.4 | 7.1 | – |
| $N_{side\ chain}$ | 20.2 | 20.8 | 0.0 |
| $a_1$–$y_1$ pathway | | | |
| TS | 37.2 | 38.3 | 43.7 |
| PBD | 13.4 | 13.0 | 17.7 |
| $a_1$ and H–Asn–OH | 39.8 | 43.9 | 50.2 |
| $y_1$-ion | 37.1 | 33.5 | 34.5 |
| $NH_3$-loss pathway | | | |
| TS | 31.2 | 35.4 | 40.7 |
| PBD | 14.5 | 24.2 | 18.7 |
| $[MH–NH_3]^+ + NH_3$ | 32.7 | 38.7 | 26.4 |

pathways are charge-directed (i.e., proton-driven) fragmentation channels, which require mobilization of the ionizing proton to the moiety to be cleaved, e.g., to the backbone or side chain amide bonds, respectively. Mobilization of the extra proton requires at least 2.0 and 1.1 kcal/mol internal energies (Table 1) to reach the backbone amide oxygens for H–Val–Asn–OH and H–Val–Gln–OH, respectively. Much more energy has to be imparted to the peptide ions to populate the backbone amide nitrogen protonated species at 15.0 and 12.9 kcal/mol relative energies for H–Val–Asn–OH and H–Val–Gln–OH, respectively (Table 1, Scheme 2). The energetics presented in Table 1 clearly show that protonation at the side chain amide oxygens and nitrogens is energetically more demanding than protonation of the corresponding backbone functionalities. For example, the relative energy of the side chain nitrogen protonated H–Val–Asn–OH species is 20.2 kcal/mol, while the corresponding backbone nitrogen protonated structure is at 15.0 kcal/mol relative energy.

Our calculations indicate that the most favored ammonia-loss pathways are initiated from side chain amide nitrogen protonated isomers (for H–Val–Asn–OH and H–Val–Gln–OH at 20.2 and 20.8 kcal/mol relative energies, respectively). Nucleophilic attack of the backbone amide oxygen on the side chain carbonyl carbon initiates elimination of $NH_3$ and formation of the lactone ring (TSs at 31.2 and 35.4 kcal/mol relative energies for H–Val–Asn–OH and H–Val–Gln–OH, respectively). It is worth noting here that we also have investigated the deamidation pathway involving the N-terminal amino group as the attacking nucleophile. This pathway is hindered by the large ring strain introduced by the *trans* backbone amide bond [29] and will not be discussed here. The deamidation pathways of protonated H–Val–Asn–OH and H–Val–Gln–OH involve TSs and product ions with six- and seven-membered rings, respectively (Figs. 2a, b). Formation of the six-membered ring for H–Val–Asn–OH is both energetically and entropically favored as compared to the seven-membered ring formed for H–Val–Gln–OH (Tables 1, 2). This indicates that deamidation is more facile for protonated H–Val–Asn–OH than for H–Val–Gln–OH.

Fragmentation to form $a_1$ and $y_1$ ions on the $a_1$–$y_1$ pathway involves backbone amide nitrogen protonated species (15.0 and 12.9 kcal/mol relative energies for H–Val–Asn–OH and H–Val–Gln–OH, respectively) as intermediates (Scheme 2). Carbon monoxide is eliminated by concerted cleavage of the amide and the $C_\alpha$–$C_{carbonyl}$ bonds via transition structures at 37.2 and 38.3 kcal/mol relative energies for H–Val–Asn–OH and H–Val–Gln–OH, respectively. While these relative energies are rather close to each other, the corresponding TSs are clearly different in terms of charge stabilization. While for H–Val–Asn–OH, both backbone as well as side chain nucleophiles stabilize the positive charge (Fig. 2c), for H–Val–Gln–OH the side chain does not take part in charge solvation (Fig. 2d). The calculated activation entropies are comparable for H–Val–Asn–OH and H–Val–Gln–OH at 9.7 and 9.3 cal/K mol, respectively.

The deamidation and the $a_1$–$y_1$ TSs of H–Val–Asn–OH and H–Val–Gln–OH represent 'text-book' examples of 'tight' and 'loose' type of reactions. Being a rearrangement, the 'tight' deamidation pathway is much more favored at low internal energies due to its lower activation energy. The 'loose' $a_1$–$y_1$ pathway becomes competitive only at higher internal energies because it is entropically favored over the deamidation (H–Val–Asn–OH: $\Delta S_{act}$ ($a_1$–$y_1$) = 9.7, $\Delta S_{act}(NH_3)$ = 0.6 cal/K mol; H–Val–Gln–OH: $\Delta S_{act}(a_1–y_1)$ = 9.3, $\Delta S_{act}(NH_3)$ = −3.4 cal/K mol). These results are in line with Harrison's CID results [27] on protonated H–Xxx–Gln–OH (Xxx involves Gly, Ala, and Val), which show that under low-energy conditions, loss of ammonia is significant, while under higher energy CID conditions, the $a_1$–$y_1$ channel becomes dominant.

As described above, the experimentally observed $\log(a_1/y_1)$ abundance ratio for protonated H–Val–Gln–OH is much larger than is predicted by Eq. (1) and the PA data of the fragments formed on the $a_1$–$y_1$ pathway. On the other hand, the experimental H–Val–Asn–OH $\log(a_1/y_1)$ ratio can reasonably be approximated by using Eq. (1). Our theoretical data on the energetics and kinetics of the $a_1$–$y_1$ and deamidation pathways provide a plausible explanation

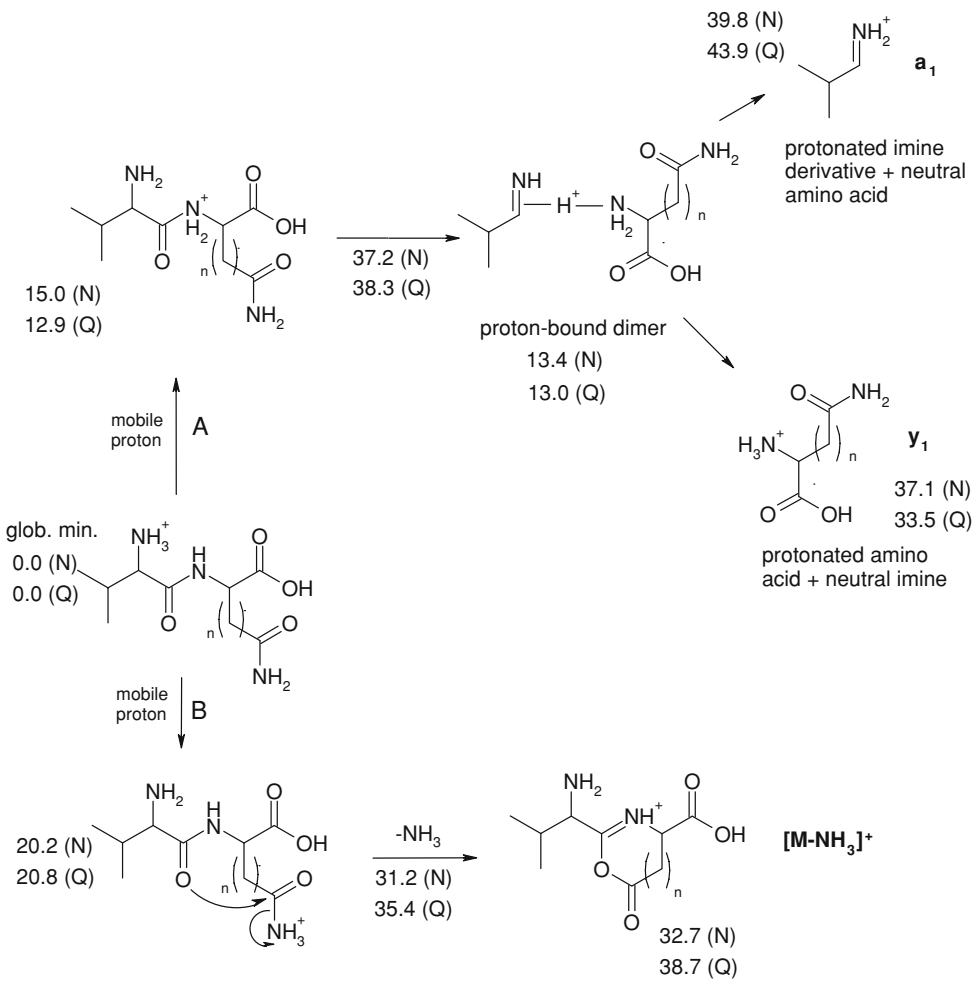


**Scheme 2** Major fragmentation reactions studied for protonated H–Val–Asn–OH and H–Val–Gln–OH, respectively, including the $a_1$–$y_1$ (A) and deamidation (B) pathways. $n$ equals 1 and 2 for H–Val–Asn–OH (noted by 'N') and H–Val–Gln–OH (noted by 'Q'), respectively. Relative energies of the investigated minima, transition states and separated products are given in kcal/mol

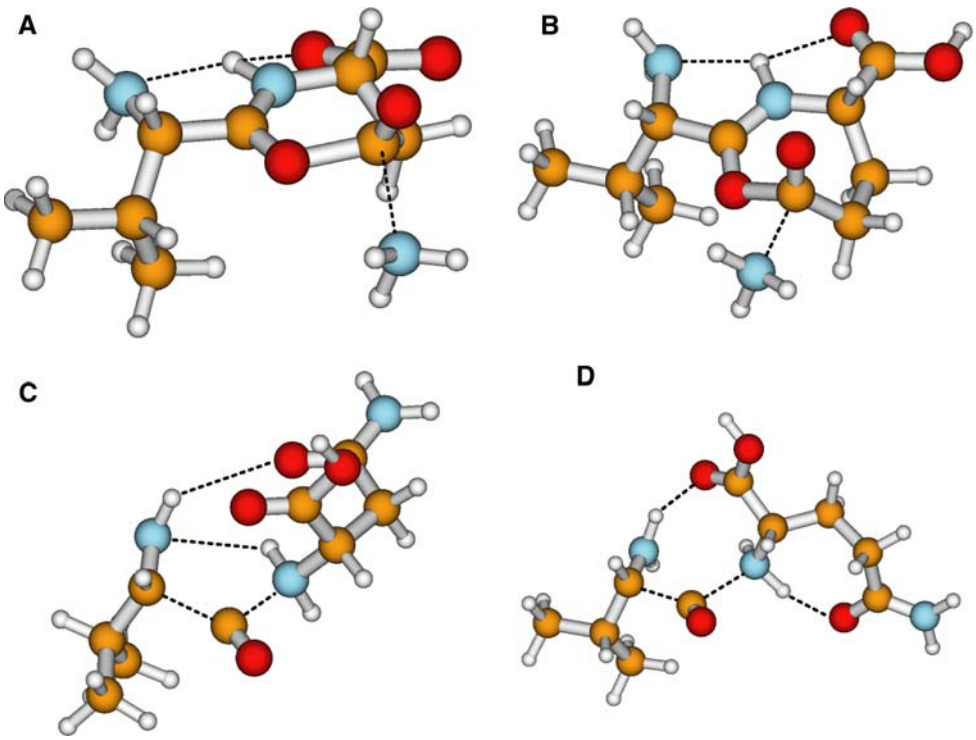


**Fig. 2** Transition structures for the deamidation (**a**, **b**) and $a_1$–$y_1$ (**c**, **d**) pathways for H–Val–Asn–OH and H–Val–Gln–OH, respectively

**Table 2** Entropies of activation $\Delta S_{act}$ (298.15 K) for the major fragmentation pathways of H–Val–Asn–OH, H–Val–Gln–OH and H–Val–Lys–OH. Values are given in cal/mol K

| | H–Val–Asn–OH | H–Val–Gln–OH | H–Val–Lys–OH |
|---|---|---|---|
| $a_1$–$y_1$ | 9.7 | 9.3 | 13.3 |
| $NH_3$ loss | 0.6 | −3.4 | 7.4 |
| $H_2O$ loss (oxazolone) | | | 4.2 |
| $H_2O$ loss (caprolactam) | | | −1.1 |

for these observations. First, we note that there is only one reaction pathway leading to $a_1$ and $y_1$ ions for protonated H–Val–Asn–OH and H–Val–Gln–OH. This is important because other competing pathways forming these ions could no doubt influence the $a_1/y_1$-ratio. Therefore, $\log(a_1/y_1)$ is unambiguously determined by the dissociation kinetics of the proton-bound dimers (PBDs) formed on the $a_1$–$y_1$ pathways of protonated H–Val–Asn–OH and H–Val–Gln–OH.

To understand the observed kinetic effects, one has to asses the major factors that determine the internal energy, equilibration and lifetime of these PBDs [10]. There is a linear relationship between the mean internal energies of peptide ions fragmenting on the $a_1$–$y_1$ pathway and those of the resulting PBDs: more energized fragmenting parent ions will lead to more energized PBDs. In other words, fragmenting species traversing TSs with higher threshold energies will produce PBD populations with higher internal energies. The mean internal energy of the PBDs has a major effect on the extent of proton equilibration [10] of the PBD and the lifetime of these species. For example, PBDs with low internal energies are expected to undergo numerous proton transfers leading to full proton equilibration before dissociation. On the other hand, highly energized PBDs can dissociate without undergoing extensive proton equilibration due to their short lifetime. As a consequence, for highly energized PBD populations the observed fragment ratio will be biased toward that particular ion holding the extra proton during the TS.

Our results indicate that deamidation is more facile at lower excitation energies than amide bond cleavage on the $a_1$–$y_1$ pathway for both H–Val–Asn–OH and H–Val–Gln–H. This means that mildly excited parent ions fragment nearly exclusively by losing ammonia, and only more strongly excited peptide ions will dissociate to form $a_1$ and $y_1$ ions. In other words it is predominantly the higher energized parent ions that fragment on the $a_1$–$y_1$ pathway, because the facile deamidation pathway is highly competitive at low excitation. This effect seems to be more pronounced for H–Val–Gln–H than for H–Val–Asn–OH. The consequence is that the average internal energy of PBDs formed on the $a_1$–$y_1$ pathway from H–Val–Gln–H is much higher than that of H–Val–Asn–H PBDs, which results in less efficient proton equilibration and a shorter PBD lifetime in H–Val–Gln–H. It follows that the corresponding $a_1$ fragment is created with higher abundance for H–Val–Gln–H than is expected, because the extra proton is located at the forming imine in the $a_1$–$y_1$ TS.

### 3.2 Fragmentation pathways of protonated H–Val–Lys–OH

The product ion spectrum of protonated H–Val–Lys–OH [8] shows a variety of fragmentation reactions leading to $a_1$ (*m/z* 72, 3.16%), $y_1$ (*m/z* 147, 100%), $[MH–NH_3]^+$ (*m/z* 229, 24.2%), $[MH–H_2O]^+$ (*m/z* 228, 71.6%), *m/z* 129 (125%) and *m/z* 101 (23.6%) ions. These fragment ion abundances are determined by a competition of the $a_1$–$y_1$, deamidation and water-loss pathways (Scheme 3). Relative energies of various protonated forms and TSs are collected in Table 3, while calculated activation entropies are presented in Table 2.

Harrison's studies on the fragmentation chemistry of protonated lysine and small peptides containing lysine demonstrated that loss of ammonia involves the side chain amino group [30]. In the following, we assume that the same holds for the ammonia loss of protonated H–Val–Lys–OH and will investigate only $S_N2$-type [31] fragmentation channels. The energetically most favored ammonia-loss pathway of protonated H–Val–Lys–OH (Scheme 3) is initiated by nucleophilic attack of the amide oxygen on the $C_{ipso}$ carbon adjacent to the protonated side chain amino group. The transition state (Fig. 3a, 40.7 kcal/mol relative energy) as well as the resulting product ion (26.4 kcal/mol relative energy) contain eight-membered rings. The ammonia-loss pathways initiated by nucleophilic attack of the N-terminal amino group is disfavored both energetically and entropically and no further details will be given here. It is to be noted here that DFT calculations frequently underestimate the threshold energies of $S_N2$-type reactions [32, 33]. Therefore, our threshold value for the ammonia loss must be considered as lower bound for the actual threshold. We did not perform more accurate MP2 calculations to determine the $S_N2$-type ammonia-loss barrier since this reaction does not influence the observed $a_1/y_1$ ratio for protonated H–Val–Lys–OH (for more details, see below).

Of the three dipeptides studied in this work, H–Val–Lys–OH had the highest $a_1$–$y_1$ (Scheme 3, Fig. 3b) energy barrier at 43.7 kcal/mol. The most abundant peak in the product ion spectrum of protonated H–Val–Lys–OH belongs to formation of *m/z* 129, which is commonly observed [34] for Lys-containing peptides. The *m/z* 129

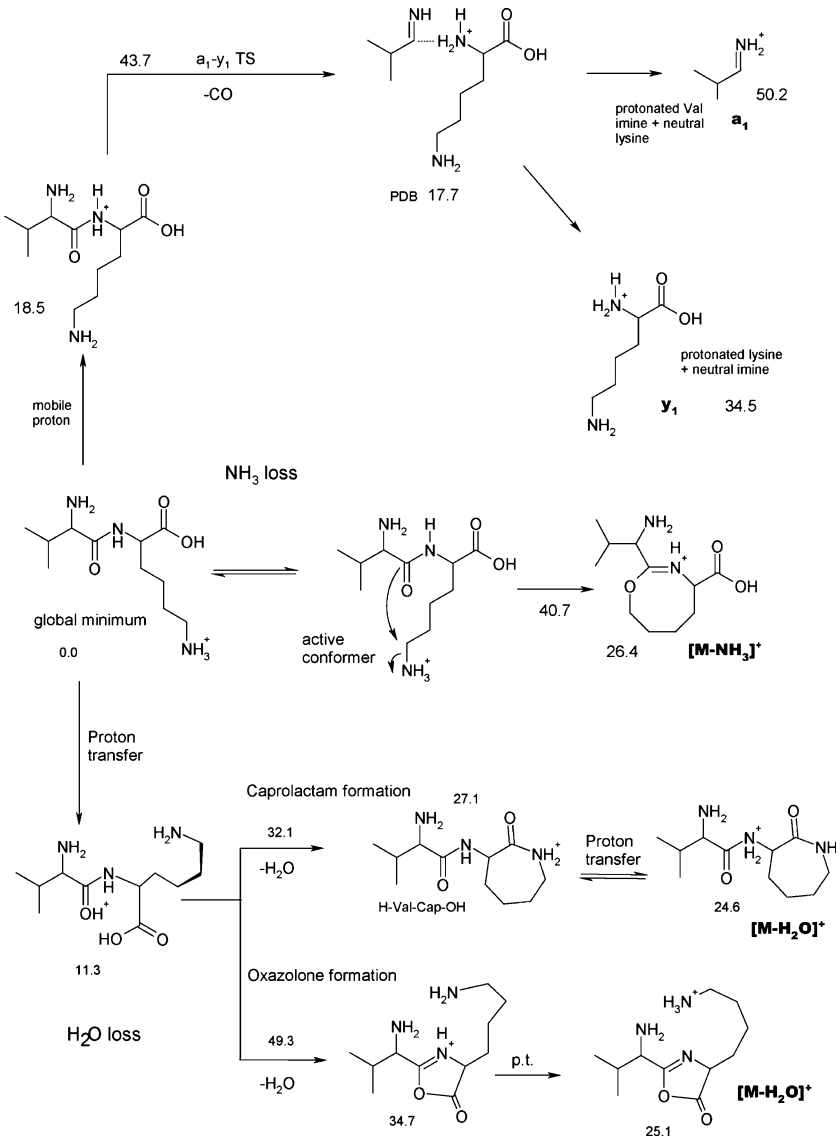


**Scheme 3** Major fragmentation pathways of protonated H–Val–Lys–OH including the $a_1$–$y_1$, deamidation and water-loss channels

**Table 3** Relative energies (kcal/mol, corrected for ZPE) with respect to the global minimum for species occurring along water-loss pathways (specific to protonated H–Val–Lys–OH)

| | |
|---|---|
| $H_2O$ loss to form the oxazolone isomer of $[MH–H_2O]^+$ | |
| TS | 49.3 |
| $[MH–H_2O]^+ + H_2O$ | 25.1 |
| $H_2O$ loss leading to protonated caprolactam and $a_1$ ions | |
| 1. H–Val–Cap–OH-formation | |
| TS | 32.1 |
| H–Val–Cap–$OH_{Cap}$ | 27.7 |
| H–Val–Cap–$OH_{amide\ N}$ | 25.2 |
| 2. $a_1$-$y_1$-like fragmentation of H–Val–Cap–OH | |
| TS | 44.6 |
| $a_1$ and α-amino-ω-caprolactam | 51.3 |
| Protonated α-amino- ω-caprolactam and i-pr-imine | 47.2 |

peak is also observed in the MI mass spectrum of H–Lys–OH [34], however, at much lower abundance than for H–Val–Lys–OH. Additionally, protonated H–Lys–OH fragments by eliminating ammonia to form a peak at *m/z* 130, which is not observed for H–Val–Lys–OH. This suggests that the fragment at *m/z* 129 for H–Val–Lys–OH is not formed by dissociation of the $y_1$ ion.

The peaks $[MH–H_2O]^+$, *m/z* 129 and *m/z* 101 are attributed [34] to a series of sequential fragmentation reactions presented in Schemes 3 and 4. There are many possibilities for the initial water loss from H–Val–Lys–OH depending on the protonation site and the attacking nucleophile involved. We discuss here the two most favored water-loss pathways, which both initiate from species protonated on the backbone amide oxygen (Scheme 3).

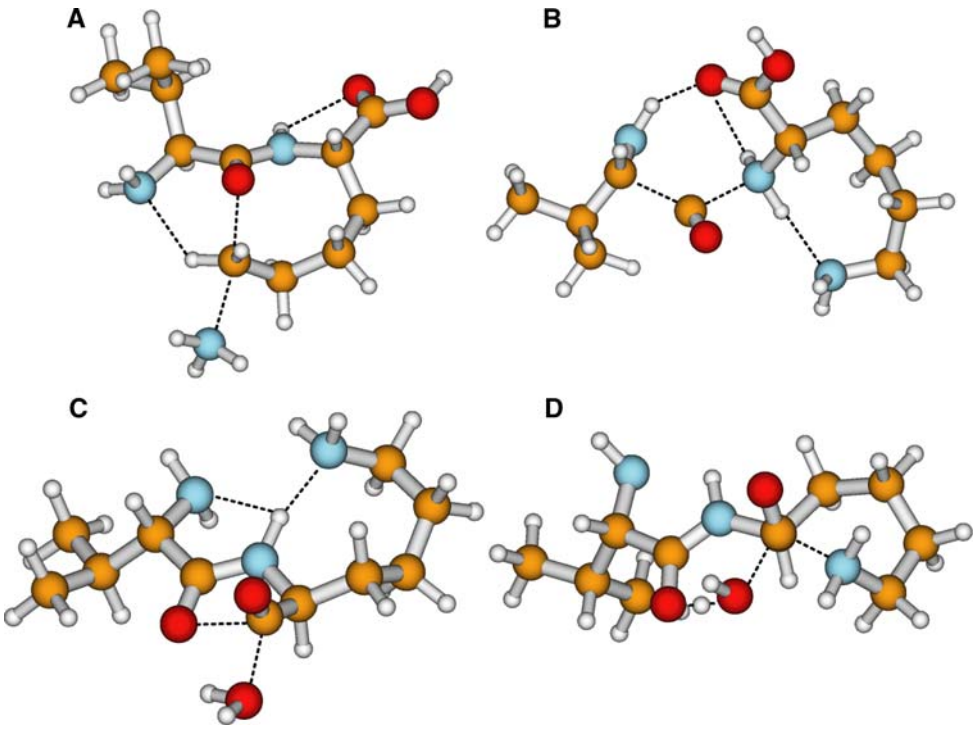


**Fig. 3** Transition structures on the (**a**) deamidation, (**b**) $a_1$–$y_1$, (**c**) oxazolone water loss, and (**d**) Lys side chain-initiated water-loss pathways of protonated H–Val–Lys–OH

Attack of the backbone amide oxygen (Fig. 3c, TS at 49.3 kcal/mol relative energy) on the carbon center of the COOH group leads to formation of an oxazolone derivative [35]. This nucleophilic attack is closely followed by a proton transfer to the hydroxyl group to form the leaving water molecule. In an energetically and entropically more favored reaction, the carbon center of the terminal COOH group is attacked by the Lys side chain amino group leading to a caprolactam derivative. Passing the corresponding TS (relative energy at 32.1 kcal/mol, Fig. 3d), the backbone amide oxygen, the COOH group and the side chain amino group interact concertedly, albeit not synchronously. The product ion thus created contains an $\omega$-caprolactam at the C-terminus and therefore is referred to as protonated H–Val–Cap–OH in the following.

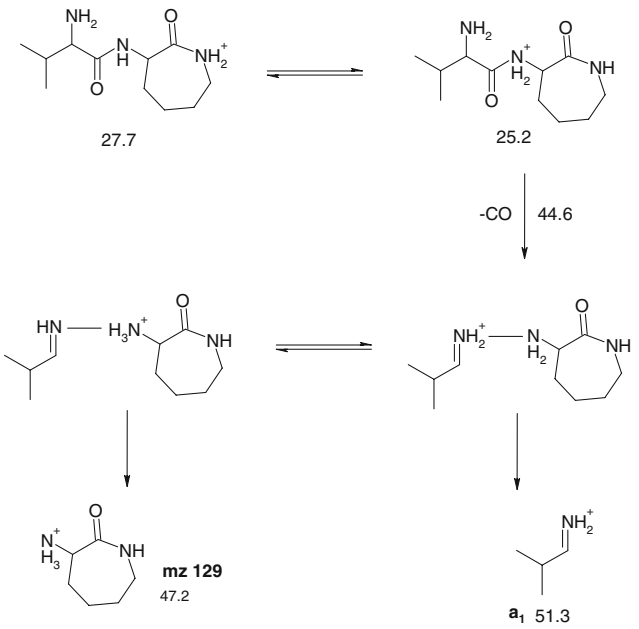


**Scheme 4** Dissociation of protonated H–Val–Cap–OH resulting in $a_1$ ions and protonated α-amino-$\omega$-caprolactam (a peak at $m/z$ 129)

The H–Val–Cap–OH species formed on water loss (Schemes 3, 4) is originally protonated at the caprolactam ring nitrogen. The ionizing proton can exothermically transfer to the backbone amide nitrogen (Fig. 4a; Scheme 4). This species can undergo an $a_1$–$y_1$-like decomposition (Fig. 4b, relative energy at 44.6 kcal/mol) producing either $a_1$ ions or protonated α-amino-$\omega$-caprolactam at $m/z$ 129 via proton-bound dimers (Scheme 4). Abundant formation of $m/z$ 129 for lysine-containing peptides has already been attributed to the formation of protonated α-amino-$\omega$-caprolactam [34]. Our theoretical data indicate that dissociation of protonated H–Val–Cap–OH provides also $a_1$ ions. The formation of $m/z$ 101 is attributed to further fragmentation of protonated α-amino-$\omega$-caprolactam [34].

Considering the competition of the $a_1$–$y_1$, $NH_3$ loss and $H_2O$-loss pathways, one can qualitatively rationalize the product ion spectrum of protonated H–Val–Cap–OH. Water loss is the far most favored pathway (relative energy of the TS at 32.1 kcal/mol), which explains the high

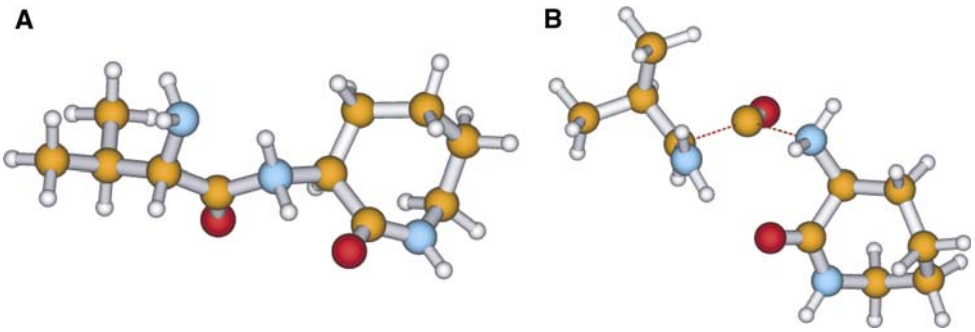


**Fig. 4** Structures of (**a**) amide nitrogen protonated H–Val–Cap–OH and (**b**) its $a_1$–$y_1$ transition structures

abundance of fragment ions generated via the water-loss sequence ($[MH–H_2O]^+$, *m/z* 129 and *m/z* 101). The relative energy of the $a_1$–$y_1$ TS is 43.7 kcal/mol, which suggests that this pathway is not competitive to the water-loss channel at low excitation energies. On the other hand, the $a_1$–$y_1$ pathway is more favored entropically ($\Delta S_{act}$ of 13.3 cal/mol K) than loss of water ($\Delta S_{act}$ of −1.1 cal/mol K) and therefore the former becomes more and more competitive at higher energies. As discussed above, our DFT calculations likely underestimate the threshold energy of ammonia loss, which is not competitive with the $[MH–H_2O]^+$ and $a_1$–$y_1$ channels if a more realistic, higher than 40 kcal/mol threshold energy is considered.

As discussed, the PA of i-pr-imine (221.7 kcal/mol) is much lower than that of Lys (235.8 kcal/mol) [25, 26]. Such a large difference in PA suggests that virtually no $a_1$ ions should be observed on the $a_1$–$y_1$ pathway when fragmenting H–Val–Lys–OH. However, Harrison et al. did observe a weak $a_1$ peak in the product ion spectrum of this peptide. One can reasonably explain this observation by considering fragmentation of protonated H–Val–Cap–OH formed by water loss from protonated H-–Val–Lys–OH. As shown in Scheme 4, this reaction leads to a proton-bound dimer of α-amino-ω-caprolactam and i-pr-imine, which then dissociates forming either protonated α-amino-ω-caprolactam or $a_1$ ions. The ratio of $a_1$ and α-amino-ω-caprolactam abundances can be approximated by Eq. (1) utilizing the PAs of the competing species. The computed PA of α-amino-ω-caprolactam is 226.9 kcal/mol, lower than that of Lys (235.8 kcal/mol), but higher than the PA of i-pr-imine (221.7 kcal/mol). These PA values suggest that $a_1$ ions are generated by fragmentation of protonated H–Val–Cap–OH. We have amended the $\log(a_1/y_1)$ versus amino acid PA plot in Fig. 1 by plotting $\log(a_1/(\text{abundance of } m/z \text{ 129}))$ versus the PA of α-amino-ω-caprolactam. This new point is clearly very close to the fitted linear free energy relationship indicating that $a_1$ ions are formed by dissociation of protonated H–Val–Cap–OH. This also suggests that relating fragment abundance ratios to PA values can be misleading if multiple channels form the corresponding ions, as is the case for $a_1$ of H–Val–Lys–OH.

## 4 Conclusions

In this study, we have investigated the fragmentation chemistry of protonated H–Val–Asn–OH, H–Val–Gln–OH and H–Val–Lys–OH by means of computational methods. The $\log(a_1/y_1)$ values observed for these peptides deviate from the general tendency observed for other H–Val–Xxx–OH peptides. While the fragmentation of other peptides in this series can be characterized by a close to linear $\log(a_1/y_1)$ versus PA(H–Xxx–OH) relationship, this is not valid for H–Val–Asn–OH, H–Val–Gln–OH and H–Val–Lys–OH [8]. It is demonstrated that considering the correct PA value for H–Asn–OH eliminates the deviation observed for H–Val–Asn–OH. The larger than expected $\log(a_1/y_1)$ value of H–Val–Gln–OH is explained by considering the dissociation kinetics of the proton-bound dimers formed on the $a_1$–$y_1$ pathway and competition of the deamidation and $a_1$–$y_1$ channels. For H–Val–Lys–OH, it is proposed that $a_1$ ions are indeed formed from one of the primary products, protonated H–Val–Cap–OH.

**Acknowledgments** BP is grateful for the financial support from the DFG (SU 244/3-1). CB is grateful for a fellowship of the DKFZ International Ph.D. Program.

## References

1. Aebersold R, Goodlett DR (2001) Chem Rev 101:269
2. Paizs B, Suhai S (2005) Mass Spectrom Rev 24:508
3. Paizs B, van Stipdonk M (2008) J Am Soc Mass Spectrom 19:1717 and papers in this focus issue on peptide fragmentation
4. Roepstorff P, Fohlmann J (1984) J Biomed Mass Spectrom 11:601
5. Biemann K (1988) Biomed Environ Mass Spectrom 16:99
6. Morgan DG, Bursey MM (1994) Org Mass Spectrom 29:354
7. Morgan DG, Bursey MM (1995) J Mass Spectrom 30:595
8. Harrison AG, Csizmadia IG, Tang TH, Tu YP (2000) J Mass Spectrom 35:683
9. Paizs B, Suhai S (2001) Rapid Commun Mass Spectrom 15:651
10. Paizs B, Schnölzer M, Warnken U, Suhai S, Harrison AG (2004) Phys Chem Chem Phys 6:2691
11. Wysocki VH, Tsaprailis G, Smith LL, Breci LA (2000) J Mass Spectrom 35:1399
12. Paizs B, Suhai S (2002) Rapid Commun Mass Spectrom 16:1699
13. Cooks RG, Kruger TL (1977) J Am Chem Soc 99:1279

14. McLuckey SA, Cameron D, Cooks RG (1981) J Am Chem Soc 103:1313
15. Harrison AG (1999) J Mass Spectrom 34:577
16. Pingitore F, Polce MJ, Wang P, Wesdemiotis C, Paizs B (2004) J Am Soc Mass Spectrom 15:1025
17. Wyttenbach T, Paizs B, Barran P, Breci L, Liu D, Suhai S, Wysocki VH, Bowers MT (2003) J Am Chem Soc 125:13768
18. Paizs B, Suhai S (2004) J Am Soc Mass Spectrom 15:103
19. Polfer NC, Oomens J, Suhai S, Paizs B (2005) J Am Chem Soc 127:17154
20. Harrison AG, Young AB, Bleiholder C, Suhai S, Paizs B (2006) J Am Chem Soc 128:10364
21. Polfer NC, Oomens J, Suhai S, Paizs B (2007) J Am Chem Soc 129:5887
22. Bleiholder C, Osburn S, Williams TD, Suhai S, Van Stipdonk M, Harrison AG, Paizs B (2008) J Am Chem Soc 130:17774
23. Case DA et al AMBER 99, University of California, San Francisco
24. Frisch MJ et al (1995) Gaussian, Inc., Pittsburgh PA
25. Bleiholder C, Suhai S, Paizs B (2006) J Am Soc Mass Spectrom 17:1275
26. Harrison AG (1997) Mass Spectrom Rev 16:201
27. Harrison AG (2003) J Mass Spectrom 38:174
28. Heaton AL, Armentrout PB (2009) J Am Soc Mass Spectrom 20:852
29. Paizs B, Suhai S (2001) Rapid Commun Mass Spectrom 15:2307
30. Dookeran NN, Yalcin T, Harrison AG (1996) J Mass Spectrom 31:500
31. Csonka IP, Paizs B, Lendvay G, Suhai S (2001) Rapid Commun Mass Spectrom 15:1457
32. Laerdahl JK, Uggerud E (2002) Int J Mass Spectrom 214:277
33. Gritsenko OV, Ensing B, Schipper PRT, Baerends EJ (2000) J Phys Chem A 104:8558
34. Yalcin T, Harrison AG (1996) J Mass Spectrom 31:1237
35. Balta B, Aviyente V, Lifshitz C (2003) J Am Soc Mass Spectrom 14:1192